Impurities in long-pulse operation of W7-X

IOP Publishing Plasma Phys. Control. Fusion 68 (2026) 035022 https://doi.org/10.1088/1361-6587/ae51c1

Plasma Physics and Controlled Fusion

PAPER

Impurities in long-pulse operation of W7-X

Monika Kubkowska[1], Marcin Jakubowski[2], Tomasz Fornal[1,*], Maciej Krychowiak[2], Andreas Dinklage[2], Marta Gruca[1], Slawomir Jablonski[1], Lukasz Syrocki[1], Birger Buttenschoen[2], Felix Reimold[2], Yu Gao[2], Golo Fuchert[2], Samuel Lazerson[2], Dirk Naujoks[2], Ulrich Neuner[2], Olaf Grulke[2], Victoria Winters[2], Daihong Zhang[2] and the W7-X Team[3]

[1] Institute of Plasma Physics and Laser Microfusion, Hery 23, 01-497 Warsaw, Poland
[2] Max-Planck-Institut für Plasmaphysik, 17491 Greifswald, Germany
[3] See Grulke *et al* 2024 (https://doi.org/10.1088/1741-4326/ad2f4d) for the W7-X Team.
[*] Author to whom any correspondence should be addressed.

E-mail: tomasz.fornal@ifpilm.pl

Keywords: stellarator, steady-state, long-pulse operation, plasma impurities

OPEN ACCESS

RECEIVED
12 November 2025

REVISED
15 February 2026

ACCEPTED FOR PUBLICATION
13 March 2026

PUBLISHED
23 March 2026

Abstract

The Wendelstein 7-X (W7-X) aims to demonstrate that the HELIAS line of stellarators can achieve high power and high performance under steady-state conditions. Such a scenario makes stellarators attractive candidates for fusion reactors offering potentially lower operating costs for continuously operated power plants. Therefore, a number of experiments have been performed at W7-X to demonstrate long-pulse operation. During the operational phase 1.2 (OP1.2) at W7-X, which took place in 2017–2018, a 100 s discharge with attached divertor plasmas was achieved, while the detached conditions were sustained for about 27 s. Performed experiments showed that a robust detachment scenario allows to reduce the peak heat flux by almost an order of magnitude and no significant increase of impurity concentration was observed (with $Z_{\mathrm{eff}} < 1.5$). The pulse duration was limited by the thermal limits of inertially (non active) cooled carbon divertor configuration. In operational phase OP2.1, the installation of a new actively water-cooled carbon-fiber composite divertor allowed a significant extension of pulse operation. The longest attached discharge lasted 8 min reaching 1.3 GJ energy throughput. In this experiment, attached plasma was heated with an average of 2.7 MW of ECRH power. The longest detachment phase in OP2.1 was achieved with feed-forward Ne seeding, which kept peak heat flux at the very low level, almost everywhere below 0.5 MW m^{-2}. As a consequence, no significant increase of impurity concentration occurs with the cooler plasma boundary, and the Z_{eff} stayed below 2. The spectroscopic observation confirms that there is no Ne accumulation in the plasma core, which is an important prerequisite for steady-state high power plasmas.

1. Introduction

Combining long-pulse operation with high performance plasmas is a key challenge in achieving an economical fusion power plant. One of the requirements is to provide a well functioning exhaust concept, that enables safe and efficient divertor operation while preventing impurities from entering the plasma core. Since most of the input power needs to be radiated away, a higher concentration of radiating impurities at the plasma edge is unavoidable. However, impurities in the plasma core increase radiation losses and cause plasma dilution, which can degrade performance or even lead to a plasma termination.

The stellarator concept, which does not require inductive current for operation, offers relatively straightforward access to long-pulse operation. Therefore, one of the main goals of Wendelstein 7-X [1, 2] (the world's largest advanced stellarator, in operation since 2015) is to demonstrate high-performance, quasi-stationary long-pulse operation with a magnetic island divertor designed to accommodate a variety of magnetic field configurations [3]. Heat and particle exhaust is performed by the so-called island divertor, where large magnetic islands at the plasma boundary intersect water-cooled divertor target

plates made of carbon-fiber composite. In the 'standard configuration', an island chain with $n/m = 5/5$ islands, provides highly efficient spreading of heat fluxes across the divertor surface.

This work focuses on studying the behavior of plasma impurities during long-pulse plasma operation. In future fusion reactors, the expected average heat loads on plasma-facing components (PFCs) are of the order of 5 MW m^{-2} [4]. In ITER and DEMO, this level will only be achieved by radiative dissipation approximately 85%–90% of the plasma input power, which can only be achieved by establishing a detached divertor via impurity seeding. In long-pulse discharges, even low concentrations of impurities can result in cumulative radiative losses, leading to plasma cooling and, in severe cases, premature termination of the discharge, e.g. through a radiation collapse in stellarators or disruption in tokamaks. Extended operation also reveals how plasma-facing materials erode and redeposit over time, influencing impurity sources and impacting the long-term integrity of PFCs. As a result, understanding impurity behavior is a key research priority, especially in the context of developing reliable steady-state operation. Research conducted at W7-X enables the investigation of key aspects relevant to fusion reactors, such as the conditions necessary to achieve a detached divertor phase or scenarios with an attached divertor which is characterized by high heat loads of up to 10–15 MW m^{-2} [5].

W7-X operation has been divided into three main phases: the first, OP1.1, with a carbon limiter configuration; the second, OP1.2, with an uncooled graphite divertor configuration; and the third operational phase, OP2, with an actively cooled graphite divertor configuration. The main impurities at W7-X are carbon (from the divertor material), oxygen (from the inner wall, adsorbed during machine venting), and boron (introduced during the boronization process). These impurities originate from the intrinsic erosion of plasma-facing materials in the divertor region and on the vessel walls [6].

There are many diagnostics dedicated to the study of impurity transport [7, 8], which provide detailed information on impurity behavior during W7-X operation including spatial and temporal evolution of impurity concentrations, charge state distributions, and the effective charge Z_{eff} [9, 10]. These diagnostics include, among others, x-ray imaging spectrometers, VUV spectrometers, bolometers, and filtered cameras, enabling the assessment of impurity sources, confinement properties, and core accumulation dynamics. The data obtained play a crucial role in validating impurity transport models and in developing strategies for impurity control in long-pulse and high-performance plasmas.

A number of experiments has been performed to date on W7-X in order to prepare long-pulse operation. During OP1.2 which took place in 2017–2018, 100 s discharge with the attached divertor plasmas was achieved while the detached conditions were maintained for approximately 30 s [5]. The experiments were the first test runs preparing further development of the steady-state scenarios, nevertheless, they showed already that a robust detachment scenario can reduce the peak heat flux by almost an order of magnitude, without a significant increase in impurity concentration. It was found that in the experiment with the attached divertor, the strong impurity influx into the scrape-off-layer (SOL) had little impact on plasma performance. In both cases, the effective charge of the plasma Z_{eff} remained low at the level of 1.5 which was confirmed by the visible spectroscopy measurements [9] and pulse height analyzer spectra [11].

2. Heat and particle exhaust at Wendelstein 7-X

As mentioned before, the main mission of W7-X is to demonstrate high power, high performance, quasi-continuous operation [2]. To realize efficient heat and particle exhaust in steady-state conditions, ten divertor units were installed in W7-X, following the helical topology of the magnetic field. These divertors are intersected by large magnetic islands at the plasma boundary, which form the basis of the island divertor concept and define the interface between the confined plasma and the PFCs [12]. In the standard magnetic configuration (5/5), its island divertor forms two strike-lines on horizontal and vertical target plates. See figure 1.

Open field lines guide heat and particles, which leave the confined plasma volume, towards the divertor targets. Hereby, the magnetic islands form a SOL characterized by a connection length on the order of 100 m, significantly longer than in tokamaks. This results from the much smaller pitch angle of magnetic field lines in the island divertor geometry, which leads to extended parallel transport paths and a stronger relative influence of cross-field transport already at electron temperatures of a few tens of eV conditions under which perpendicular transport remains negligible in conventional poloidal divertors (like in tokamaks) [12].

Research conducted at W7-X allows for the study of certain aspects relevant to fusion reactors, which are expected to operate with power fluxes of up to 5 MW m^{-2}. In stellarator-based 500 MW reactor about 85% of total heating power needs to be radiated away. As a relatively new device, W7-X is still in the process of developing its full heating capabilities. During the discussed experiments, the electron

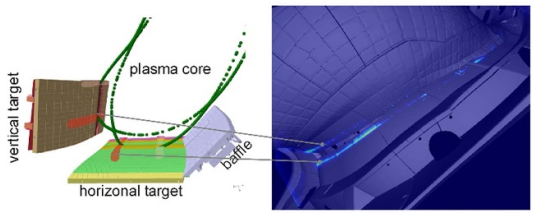

Figure 1. Illustration of two strike lines on the horizontal and vertical divertor targets in Wendelstein 7-X (left). The targets are plasma-facing components located in the divertor region of the plasma vessel, where magnetic field lines from the plasma edge intersect the material surfaces. The corresponding infrared thermography measurements of the divertor targets are shown on the right, illustrating the spatial distribution of heat loads on the target surfaces.

cyclotron resonance heating (ECRH), which is the primary heating system at W7-X [13], had available input power levels of up to ∼7 MW. Moreover, due to the large wetted areas provided by the island divertor geometry [14] and the efficient redistribution of power via impurity radiation [15], the resulting heat fluxes on the high heat flux divertor targets remain relatively low compared to reactor-relevant conditions. Under present conditions, it is not yet possible to simultaneously realize both high divertor power fluxes and high radiation fractions. Reactor-relevant power flux densities (on the order of 5–10 MW m^{-2}) can be achieved in attached plasmas, where the radiated power fraction remains modest. In contrast, when power fluxes to the divertor are reduced (typically below 1 MW m^{-2}), it becomes possible to access regimes with high radiated power fractions, leading to stable detachment over the entire divertor surface [15].

In W7-X, detachment in the island divertor is achieved either by raising the plasma density [5] (typically via density control or via the seeding of low-Z impurities such as N_2 or Ne [16]) which drives the plasma into a regime where heat and particle fluxes to the divertor targets are significantly reduced, while neutral pressure in the divertor region remains sufficiently high to sustain stable particle exhaust and density control. During detachment in the W7-X island divertor, impurity radiation (mainly from intrinsic carbon) leads to a uniform reduction of target heat fluxes by up to an order of magnitude, while the recycling particle flux decreases significantly without signs of strong volume recombination, even as divertor neutral pressure continues to rise. Additionally, the drop in electron temperature at the last closed flux surface cannot be fully explained by classical parallel heat conduction, suggesting that the detached plasma self-regulates through a complex interplay of transport channels to maintain particle, energy, and momentum balance [17].

3. Long discharges in OP1.2 experimental campaign with inertially cooled divertor

During the OP1.2 campaign, the plasma energy throughput (and thereby the achievable pulse length) was limited by the technical constraints of the uncooled divertor and plasma vessel. To avoid thermal overload of PFCs, the maximum permitted energy throughput was set to 200 MJ, effectively restricting the operational space for high-power, long-duration discharges [5]. The maximum duration of the detached scenario was 30 s with an inertially cooled carbon divertor [18], as exemplified in figure 2. Here the detachment has been achieved by raising the plasma density, which lead to enhanced concentration of carbon ions at the plasma boundary [19] and thus plasma radiation. The TDU divertor was a large net erosion source during OP1.2 [20]. During this 30 s experimental program, plasma was heated using 5 MW of ECRH, reaching a line-integrated electron density ($\int n_e dl$) of 1.1 × 10^{20} m^{-2}. Full intrinsic detachment, i.e. detachment driven by radiative cooling from naturally present (intrinsic) impurities without external impurity seeding, was achieved after 3 s. In this case the radiated power fraction exceeded 0.8 ($f_{rad} \geqslant 0.8$), while the peak divertor heat flux remained below 0.5 MW m^{-2}.

The elevated plasma radiation was kept stable thanks to an efficient feedback system available during the OP1.2 campaign [21]. Importantly, the average effective ion charge (Z_{eff}), obtained from spectroscopic bremsstrahlung measurements, remained constant at approximately 1.5, indicating no increase in impurity concentration during the discharge. The main contribution to Z_{eff} comes from carbon, as the divertor's material [5].

The last two plots on figure 2 present the temporal evolution of the main impurity spectral lines observed by the VUV spectrometer HEXOS [22]. It is clearly visible that, starting from 3 s, the intensity of carbon and oxygen lines, two of the main intrinsic impurities, increases, which contributes to

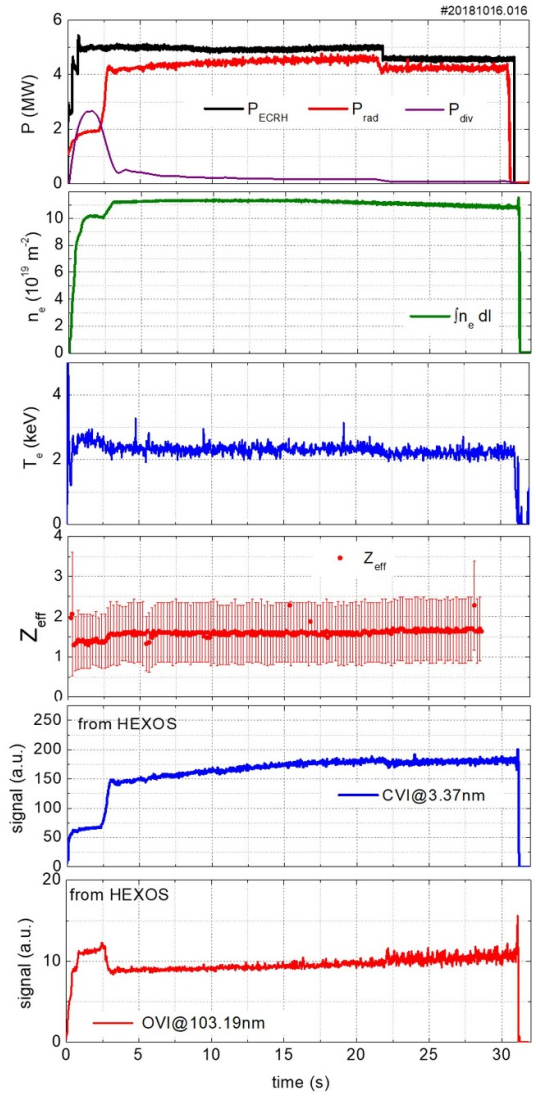

Figure 2. Plasma parameters for the longest discharge (20181016.016) obtained in the detached regime during OP1.2. From the top: total heating (P_{ECRH}), total radiated power (P_{rad}) and total divertor power (P_{div}), line-integrated electron density ($\int n_e dl$), central electron temperature (T_e), effective ion charge (Z_{eff}), smoothed time traces of carbon and oxygen spectral lines observed by the HEXOS spectrometer.

enhanced radiation in the divertor SOL, thereby cooling the plasma near the divertor plates. This increase reflects changes in local plasma conditions in the edge and SOL regions, where the HEXOS lines mainly originate, and does not imply an increase of the core impurity content. Consequently, the observed rise in impurity radiation is consistent with the approximately constant, core-dominated Z_{eff}.

The longest discharge obtained with the inertially cooled divertor in the attached regime lasted approximately 100 s. The plasma, in the high-iota magnetic configuration [3], was heated by 2 MW of ECRH, and the total energy turnover in this discharge reached approximately 200 MJ. Figure 3 presents the main plasma parameters of this discharge. The radiation fraction (f_{rad}) during the entire program was approximately 30%, resulting in a fully attached divertor plasma. As can be seen, the line-integrated electron density remained stable at the level of $\sim 3 \times 10^{19}$ m^{-2} until $t = 80$ s. As the divertor units were not water-cooled during this campaign, their surface temperatures steadily increased over the course of the discharge, exceeding 1000 °C in this program. This temperature rise enhanced impurity release (carbon from the graphite tiles and oxygen likely originating from adsorbed water layers on the target surfaces) resulting in increased plasma radiation and a rise in core density during the final phase of the discharge. The elevated temperatures, combined with intense hydrogen fluxes, are consistent with

enhanced chemical sputtering, which is known to contribute significantly to carbon erosion [20]. This observation is confirmed by both PHA and HEXOS diagnostics, as shown in figure 3. A small difference in the behavior of the CVI line at 459 eV and at 3.37 nm (368 eV) can be observed around 30 and 80 s, however, these differences are not significant. Although both lines correspond to the same ionization stage of carbon, the data are obtained from two different diagnostic systems with different lines of sight. The temporal evolution of oxygen spectral line intensity shows the increase in the last phase of the discharge, from about 80 s. Simulations with EMC3-Eirene indicate that impurity ionization in W7-X occurs primarily in regions of the island SOL where parallel transport is suppressed by friction, and that impurity leakage is mostly happening by perpendicular transport through the O-point region [23]. This is most likely the mechanism which leads here to elevated core concentration of both carbon and oxygen ions.

4. Long discharges in OP2.1 experimental campaign with actively water cooled divertor

The issue of enhanced carbon and oxygen sources during long pulse has been mitigated by very efficient boronization in the following campaigns [24], which proved to be highly effective at W7-X, leading to a substantial reduction of impurity influxes—oxygen levels at the divertor decrease typically by over two orders of magnitude after repeated applications, while carbon influx is being suppressed by a factor of four. Moreover, significant enhancement to the W7-X infrastructure were performed prior to the experimental phase OP2. This included the installation of 600 in-vessel cooling circuits, a water-cooled high-heat-flux divertor and ten identical cryo-pumps located behind each of the 10 divertor units. These enhancements allow W7-X to operate for up to 30 min with 10 MW of input power.

During the operational phase OP2.1, conducted with an actively cooled divertor configuration, ECR-heated plasmas with durations of up to 100 s were achieved, featuring stable detached divertor operation and a total plasma energy throughput of up to 350 MJ. Figure 4 presents the main plasma parameters of such program, which was performed using the standard magnetic configuration. An increase in line-integrated density to 1.35×10^{20} m^{-2} resulted in a plasma radiated power fraction exceeding $f_{\mathrm{rad}} > 0.8$, which results in the detachment of the divertor plasma. The plasma radiation is enhanced at higher density due to higher increased carbon concentration. In these discharge, the electron density was actively increased by additional gas injection. Due to the reduced influx of intrinsic impurities (carbon and oxygen) after plasma vessel boronization performed prior to this experiment, higher plasma densities were required to achieve sufficient radiative cooling. The oscillations seen in the transition period are artifacts caused by feedback controller settings [21], which affected P_{rad} and consequently altered divertor power loads. After an initial phase of unstable density control, the electron density n_{e} was maintained at the desired level for high plasma radiation via the feedback system throughout the entire discharge. The feedback system reacted to the drop of input power at $t \approx 42$ s and adjusted the plasma density accordingly. Reduced heat fluxes to the divertor during the entire detached phase resulted in low surface temperatures (150 °C–160 °C). As a consequence, no significant increase in impurity concentrations was observed in the cooler plasma boundary, and Z_{eff} remained below 2. Time traces of C VI and O V line intensities measured by HEXOS do not show any significant increase in the flat top phase.

Following a few boronization procedures prior to experiments, the intrinsic impurity content (particularly oxygen and carbon) was significantly reduced, during OP2.1 which, while beneficial for overall wall conditioning, led to a marked decrease in intrinsic detachment [25]. As a result, achieving detachment in post-boronization scenarios increasingly required the use of externally seeded impurities to compensate for the reduced radiative losses at the plasma edge. This operational shift highlights the critical role of impurity seeding, especially in future campaigns with a carbon-free first wall, where intrinsic radiation levels are expected to be even lower. Since the SOL at W7-X is expected to operate at electron temperatures ranging from a few to about 10 eV, the choice is limited to low- or medium-Z species, such as N_2 or Ne.

The longest detachment program in OP2.1 was achieved with Ne seeding. To increase the electron density, Ne was puffed every 2.5 s, which kept the radiation power (P_{rad}) baseline constant at $f_{\mathrm{rad}} = 0.8$ during the first 18 s of the discharge (see figure 5). Unfortunately, the feedback system to control plasma radiation during OP1.2 was not available during this experimental campaign. This required us to use feed-forward seeding of impurities, since spontaneous changes in plasma radiation (for instance at $t = 18$ s, when the heating power was reduced due to a gyrotron failure) could not be taken into account. Nevertheless, the plasma still remained stable, even though the plasma radiation

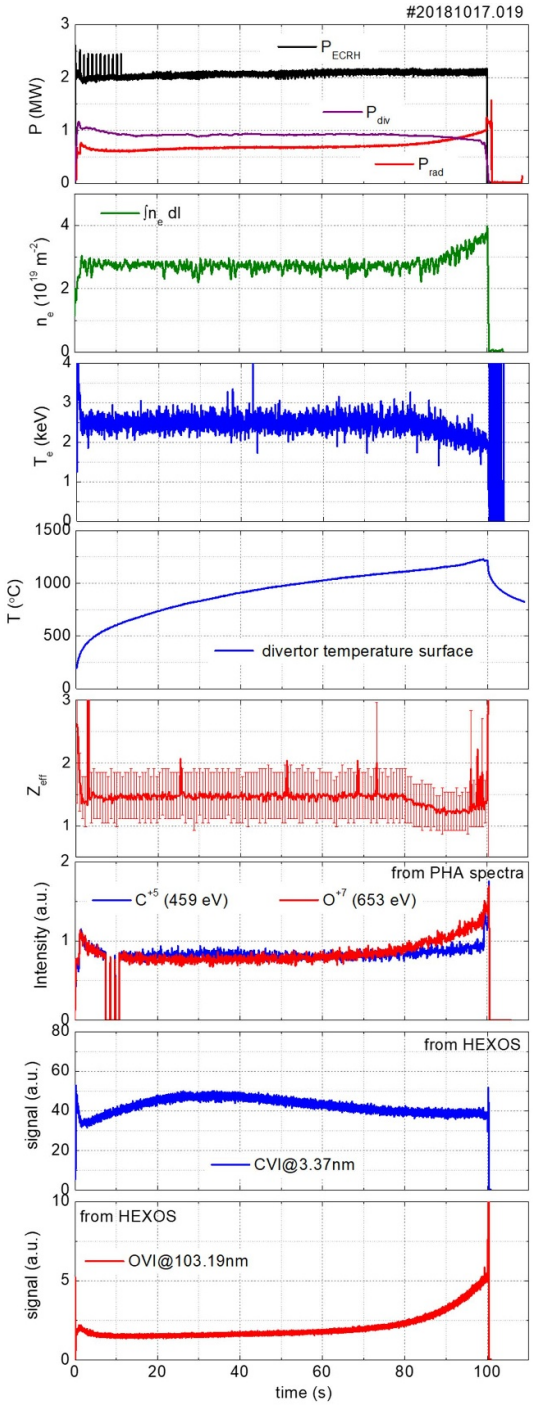

Figure 3. Plasma parameters for the longest discharge (20181017.019) obtained in the attached regime during OP1.2. From the top: total heating (P_{ECRH}), total radiated power (P_{rad}) and total divertor power (P_{div}), line-integrated electron density $\int n_e dl$ (—), central electron temperature (T_e), temperature on the divertor surface and effective ion charge (Z_{eff}), smoothed time traces of main impurity spectral lines observed by HEXOS and the PHA systems. In case of time traces of O lines observed by HEXOS, the behavior is almost the same for both lines.

reached $f_{rad} > 0.9$. The electron density remained nearly constant at a level of 1.3×10^{20} m^{-2} during the entire discharge. The snapshot on the figure 5 shows the averaged heat flux distribution on the divertor plates between 8 and 15 s. As shown, the peak heat flux during the detached phase with Ne seeding remains very low, staying almost entirely below 0.5 MW m^{-2}. This is the result of a very high radiation fraction, which typically indicates plasma detachment. In attached plasmas with similar input power, the peak heat flux would be approximately one order of magnitude higher.

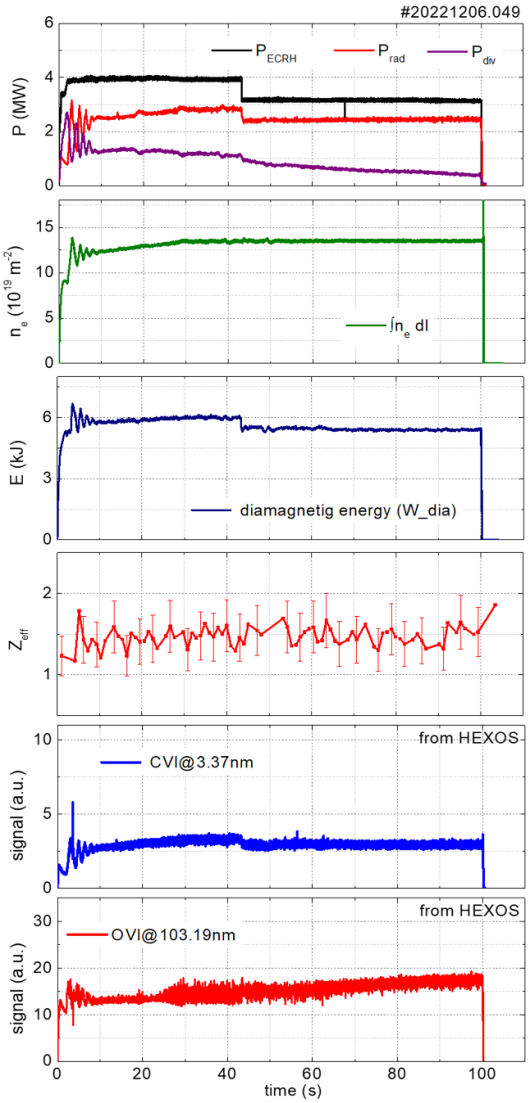

Figure 4. Plasma parameters of discharge (20221206.049), measured during OP2.1 at W7-X in the detached divertor phase. From top to bottom: total heating (P_{ECRH}), total radiated power (P_{rad}) and total divertor power (P_{div}), line-integrated electron density ($\int n_e$ dl), diamagnetic energy (W_{dia}), effective ion charge (Z_{eff}), and time smoothed traces of carbon and oxygen spectral line intensities measured by HEXOS.

Feed-forward Ne injection through the divertor gas nozzles released approximately of 8×10^{17} atoms of Ne per puff into the downstream plasma. Time traces from the HEXOS spectrometer show that the line intensities corresponding to higher ionization states of neon exhibit a characteristic oscillatory behavior with each puff (initially increasing, then stabilizing) while the overall baseline remains constant. This indicates that neon, although a low-recycling impurity, does not accumulate in the plasma core over time, a key requirement for sustained impurity seeding in steady-state, high-power scenarios. It is an important finding towards the all-metal wall of future devices.

The carbon and oxygen line intensities also indicate no significant core contamination. It has previously been demonstrated [26] that ECR-heated plasmas with electron root confinement are characterized by strong anomalous diffusion due to turbulence. In addition, divertor plasmas exhibit effective impurity retention, as exemplified by divertor overload experiments in which large amounts of carbon were eroded from the divertor target plates [5, 23].

4.1. The longest discharge during OP2.1

In OP2.1, W7-X was able to significantly increase the pulse duration of attached plasmas, reaching a total energy turnover of 1.3 GJ. For example, a plasma was heated with an average ECR heating power

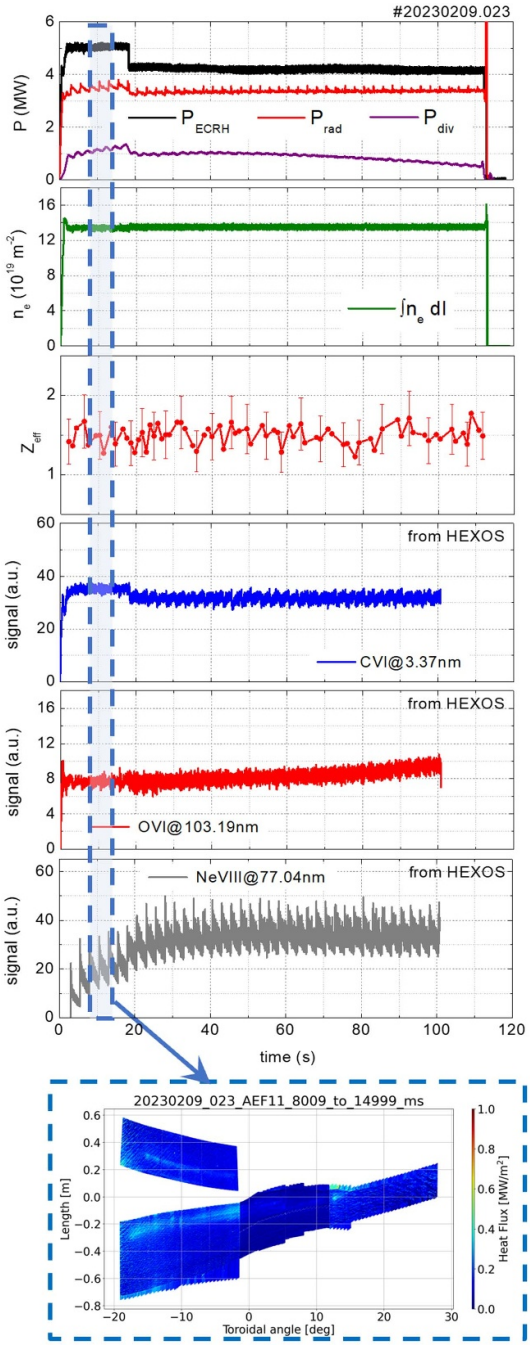

Figure 5. Plasma parameters of discharge (20230209.023), measured during OP2.1 at W7-X in the detached divertor phase. From top to bottom: total heating (P_{ECRH}), total radiated power (P_{rad}) and total divertor power (P_{div}), line-integrated electron density ($\int n_e$ dl), effective ion charge (Z_{eff}), and smoothed time traces of carbon, oxygen and neon spectral line intensities measured by HEXOS. Data are shown only up to 100 s due to an issue with the data acquisition system. Below is a snapshot of the averaged heat flux distribution on the divertor plates from infrared cameras, taken over time periods from 8 to 15 s.

of 2.7 MW over a 480 s discharge. Attached plasmas are of particular interest due to the higher power loads to the divertor, which are in the range of those expected in ITER and DEMO.

The main plasma parameters from this program are presented in figure 6. The top graph presents the time evolution of input power and total divertor power load (unfortunately, the radiated power data P_{rad} are not available due to the diagnostic system failure). The ratio of these two indicates fully attached plasma. For the first 5 min, the plasma was heated with 3 MW of ECRH; unfortunately, due to technical issues some gyrotrons started to drop out as a result of insufficient water cooling. Consequently, in the final tens of seconds, only 1.2 MW of ECRH was still used.

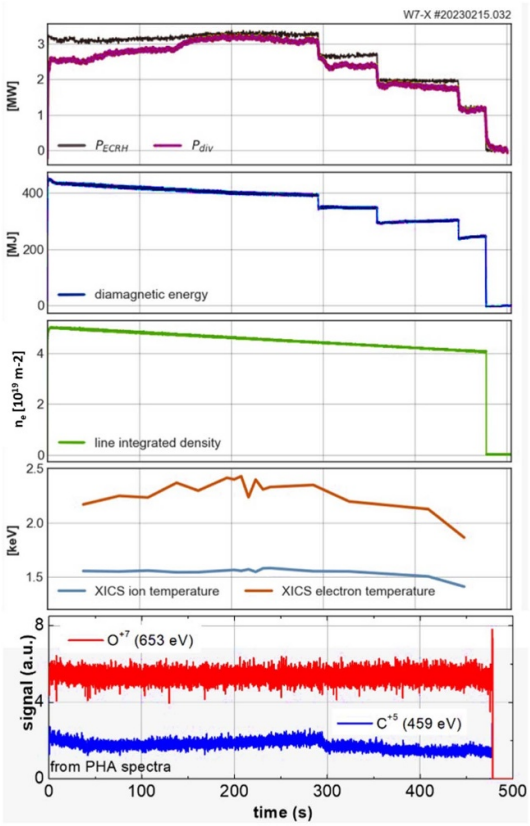

Figure 6. Time traces of the longest discharge (20230215.032) of the OP2.1. From top to bottom: total heating (P_{ECRH}—), total divertor power (P_{div}), diamagnetic energy (W_{dia}), line-integrated electron density ($\int n_e$ dl), central electron and ion temperatures from XICS, and variations in carbon and oxygen spectral line intensities measured by the PHA system.

Owing to the limited availability of impurity diagnostic data for discharge 20 230 215.032 (particularly during the long-pulse phase) an alternative discharge, 20 230 215.015, with similar plasma parameters (P_{ECRH} and n_e), was selected for the analysis of carbon and oxygen behavior, as shown in figure 7. This substitution was necessary because not all diagnostics were operational during the original discharge, preventing impurity transport modeling and a reliable estimation of Z_{eff}. The selected discharge provides representative impurity behavior under comparable conditions. The impurity concentrations were determined by simulating PHA x-ray spectra using the SimXray code [27]. The error bars were estimated at 20%, influenced by several factors, including the energy resolution of the PHA spectrometer (about 120 eV at 500 eV), the detector efficiency in the low-energy range where C and O lines are observed, and the system geometry [28, 29].

Also here, the evolution of O and C (the top panel of figure 8) concentration (expressed as a fraction of the electron density) again shows no significant accumulation of impurities in the plasma core and rather weak reaction to changes in the input power and the divertor power loads. This shows that ECRH-heated plasmas are resilient towards impurity accumulation, which comes from enhanced impurity transport in the plasma core and good impurity retention at the plasma edge. Contrary to the attached discharges in OP1.2, the divertor target plates in OP2.1 are water-cooled, making surface temperatures exceeding 1000 °C unlikely at this level of input power. Concentrations of carbon and oxygen are strongly dependent on plasma density, primarily through changes in edge and SOL transport and plasma–wall interaction [30] processes rather than enhanced core confinement, which was programmed in a feed-forward manner to gradually decrease from 5×10^{19} m^{-2} to 4×10^{19} m^{-2} over the course of the discharge.

Moreover, the Z_{eff} calculations based on the PHA spectra (see the bottom panel of figure 8) show no observable changes between the detached (red) and attached (black) divertor scenarios. The difference between these scenarios is minimal and remains within the error margins, confirming that the ECRH plasma is resilient to impurity accumulation [31, 32].

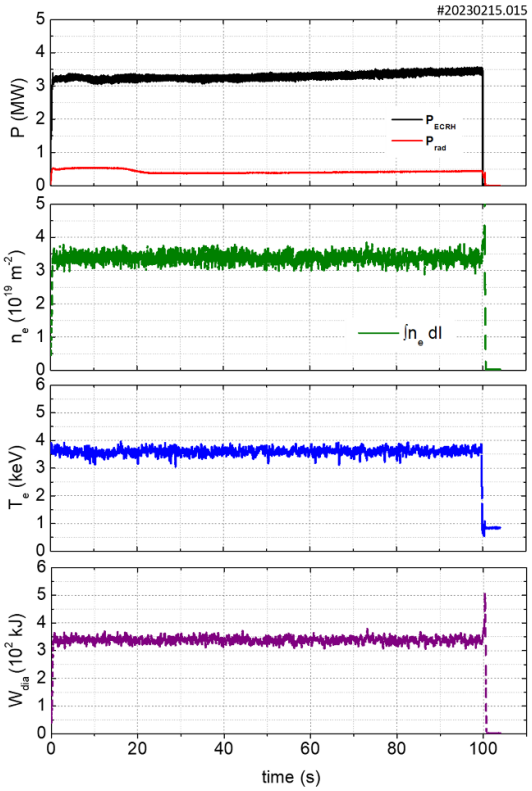

Figure 7. Time traces of discharge 20 230 215.015, which is characterized by plasma parameters similar to those of the longest discharge 20 230 215.032 of OP2.1. From top to bottom: total heating (P_{ECRH}), total radiated power (P_{rad}), line-integrated electron density ($\int n_e$ dl), central electron temperature (T_e) and diamagnetic energy (W_{dia}).

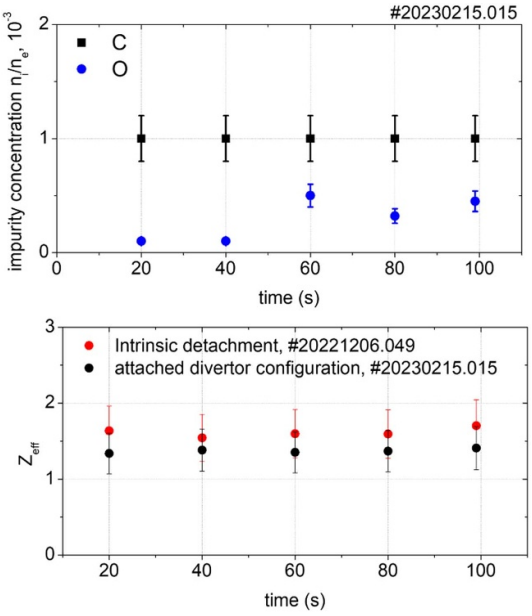

Figure 8. Evolution of carbon and oxygen concentrations (top) for chosen attached divertor configuration and Z_{eff} values (bottom) derived from simulated PHA spectra for detached (**red**) and attached (**black**) divertor regimes.

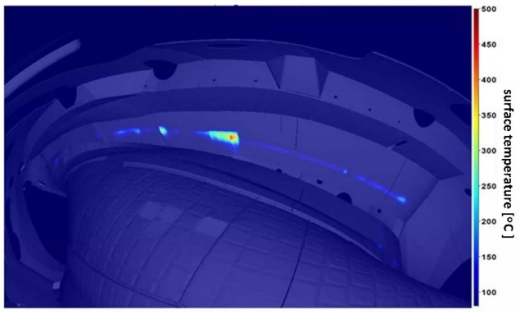

Figure 9. Infrared thermography image of the water-cooled divertor baffles in W7-X during the longest OP2.1 discharge, averaged over the full 8 min discharge duration. The plasma-divertor contact region (strike line) is clearly visible, with the color scale indicating the surface temperature of the divertor target elements.

In figure 9, which presents an infrared image of the temperature distribution on the water-cooled divertor baffles at W7-X during the longest discharge of OP2.1, the plasma-divertor contact region (so-called strike line) is clearly visible, what also confirm the attached plasma configuration. The highest temperature of the target elements reaches approximately 500 °C, which is significantly lower than the values observed for the uncooled divertor units during OP1. This of course significantly reduces chemical sputtering, in contrary to scenario with the inertially cooled divertor.

5. Summary and conclusions

The experiments conducted at W7-X have advanced the understanding of intrinsic and seeded divertor detachment in the standard magnetic configuration. To enable effective density control and improved plasma performance, a reduction of impurities and outgassing is needed. Achieving detachment requires enhanced radiation to dissipate power towards the divertor. Control of plasma radiation through impurity seeding with Ne has been demonstrated both in OP1.2 and OP2.1 W7-X experimental campaigns.

The results indicate safe and controllable long-pulse operation with the actively cooled plasma facing components recently installed at W7-X. The long-pulses were performed without impurity accumulation and no long-time-scale processes were observed that would pose a risk to stable plasma performance in the scenarios studied. While carbon and oxygen influxes increased toward the end of 100 s pulse with inertially cooled divertor (driven by thermally enhanced release) these effects could be mitigated with water-cooled plasma facing components and efficient boronizations. Importantly, there was no evidence of first-wall deterioration or evolving impurity sources that would threaten long-duration operation. A notable example is an 8 min discharge reaching 1.3 GJ of energy, fulfilling one of the major goals of the campaign with the actively water-cooled carbon divertor.

The findings imply the progress in fulfillment mission 8 of the European fusion roadmap [33], which aims to bring stellarators to maturity as a viable alternative line to fusion electricity and to establish a robust physics basis for stellarator development.

Acknowledgments

This work has been carried out within the framework of the EUROfusion Consortium, funded by the European Union via the Euratom Research and Training Programme (Grant Agreement No 101052200—EUROfusion). Views and opinions expressed are however those of the author(s) only and do not necessarily reflect those of the European Union or the European Commission. Neither the European Union nor the European Commission can be held responsible for them.

This scientific paper has been published as part of the international project co-financed by the Polish Ministry of Science and Higher Education within the programme called ‘PMW’.

Data availability statement

All data that support the findings of this study are included within the article (and any supplementary files).

Author contributions

Monika Kubkowska 0000-0003-1320-7468
Conceptualization (lead), Data curation (lead), Formal analysis (lead), Funding acquisition (lead), Investigation (lead), Methodology (lead), Supervision (lead), Validation (lead), Visualization (lead), Writing – original draft (lead), Writing – review & editing (equal)

Marcin Jakubowski 0000-0002-6557-3497
Conceptualization (equal), Data curation (equal), Formal analysis (supporting), Funding acquisition (equal), Investigation (equal), Methodology (equal), Supervision (supporting), Validation (equal), Writing – original draft (supporting), Writing – review & editing (equal)

Tomasz Fornal 0000-0002-9240-1199
Data curation (supporting), Formal analysis (equal), Investigation (supporting), Validation (supporting), Visualization (supporting), Writing – original draft (equal), Writing – review & editing (equal)

Maciej Krychowiak
Data curation (equal)

Andreas Dinklage 0000-0002-5815-8463
Conceptualization (supporting), Data curation (supporting)

Marta Gruca 0000-0001-7443-2250
Data curation (supporting)

Slawomir Jablonski
Data curation (equal), Formal analysis (equal)

Lukasz Syrocki
Data curation (supporting)

Birger Buttenschoen 0000-0002-9830-9641
Data curation (equal)

Felix Reimold
Data curation (supporting), Investigation (supporting)

Yu Gao 0000-0001-8576-0970
Data curation (equal)

Golo Fuchert 0000-0002-6640-2139
Data curation (equal)

Samuel Lazerson
Data curation (supporting)

Dirk Naujoks 0000-0003-4265-6078
Data curation (supporting)

Ulrich Neuner
Data curation (supporting)

Olaf Grulke
Data curation (supporting)

Victoria Winters 0000-0001-8108-7774
Data curation (supporting)

Daihong Zhang 0000-0002-5800-4907
Data curation (equal), Investigation (supporting)

References

[1] Bosch H-S *et al* 2017 *Nucl. Fusion* **57** 116015
[2] Klinger T *et al* 2019 *Nucl. Fusion* **59** 112004
[3] Geiger J, Beidler C D, Feng Y, Maaßberg H, Marushchenko N B and Turkin Y 2015 *Plasma Phys. Control. Fusion* **57** 014004
[4] Pitts R A *et al* 2011 *J. Nucl. Mater.* **415** S957–64
[5] Jakubowski M *et al* 2021 *Nucl. Fusion* **61** 106003

[6] Wauters T et al 2018 Nucl. Mater. Energy 17 235–41
[7] König R et al 2015 J. Instrum. 10 10002
[8] Kubkowska M et al 2018 Problems At. Sci. Technol. 118 312–6 (available at: https://vant.kipt.kharkov.ua/ARTICLE/VANT_2018_6/article_2018_6_312.pdf)
[9] Pavone A et al 2019 J. Instrum. 14 C10003
[10] Kwak S et al 2021 Rev. Sci. Instrum. 92 43505
[11] Kubkowska M et al 2018 Rev. Sci. Instrum. 89 10–111
[12] Feng Y, Kobayashi M, Lunt T and Reiter D 2011 Plasma Phys. Control. Fusion 53 024009
[13] Laqua H P et al 2021 Nucl. Fusion 61 106005
[14] Niemann H et al 2020 Nucl. Fusion 60 084003
[15] Zhang D et al 2019 Phys. Rev. Lett. 123 025002
[16] Effenberg F et al 2019 Nucl. Fusion 59 106020
[17] Feng Y et al 2021 Nucl. Fusion 61 086012
[18] Bosch H-S et al 2020 IEEE Trans. Plasma Sci. 48 1369–75
[19] Perseo V et al 2021 Nucl. Fusion 61 116039
[20] Mayer M et al 2021 Phys. Scr. 96 124070
[21] Krychowiak M et al 2023 Nucl. Mater. Energy 34 101363
[22] Buttenschön B et al 2016 43rd EPS Conf. on Plasma Physics vol P4.012 (Poster)
[23] Winters V et al 2024 Nucl. Fusion 64 056042
[24] Sereda S et al 2020 Nucl. Fusion 60 086007
[25] Wischmeier M et al 2018 27th IAEA Fusion Energy Conf. (Poster)
[26] Geiger B et al 2019 Nucl. Fusion 59 046009
[27] Jabłoński S, Czarnecka A, Kubkowska M, Ryć L, Weller A, Biedermann C and König R 2015 J. Instrum. 10 P10021
[28] Krawczyk N et al 2017 Fusion Eng. Des. 123 1006–10
[29] Kubkowska M et al 2018 Fusion Eng. Des. 136 58–62
[30] Angioni C 2021 Plasma Phys. Control. Fusion 63 073001
[31] Dux R et al 2003 Plasma Phys. Control. Fusion 45 1815
[32] Tamura N, Suzuki C, Satake S, Nakamura Y, Nunami M, Funaba H, Tanaka K, Yoshinuma M, Ida K and Sudo S 2017 Phys. Plasmas 24 056118
[33] EUROfusion Consortium n.d. European Research Roadmap to the Realisation of Fusion Energy (available at: https://euro-fusion.org/eurofusion/roadmap/) (Accessed 03 October 2025)